Spatio-Temporal Clustering of Seismicity Enabled by Off-Fault Plasticity

Md Shumon Mia[1,2], Mohamed Abdelmeguid[2], Ahmed E. Elbanna[2,3]

[1]Department of Mechanical Science and Engineering, University of Illinois at Urbana-Champaign, Urbana, IL, USA.

[2]Department of Civil and Environmental Engineering, University of Illinois at Urbana-Champaign, Urbana, IL, USA.

[3]Beckman Institute of Advanced Science and Technology, University of Illinois at Urbana-Champaign, Urbana, IL, USA.

Corresponding author: Md Shumon Mia (mmia2@illinois.edu)

Key Points:

- Sequence of earthquake and aseismic slip is simulated for a rate-and-state fault with off-fault plasticity.
- Interaction between fault slip and off-fault plasticity leads to rupture arrest and spatio-temporal clustering of seismicity.
- Plastic dissipation is a small fraction of the total energy budget but its impact is amplified by its feedback on stress heterogeneity.

Abstract

While significant progress has been made in understanding earthquake source processes in linear elastic domains, the effect of more realistic rheologies including plasticity is poorly understood. Here, we simulate sequence of earthquake and aseismic slip of a 2D antiplane rate-and-state fault embedded in a full-space elastic-plastic bulk. We show that off-fault plasticity may lead to partial ruptures as well as temporal clustering of seismic events. Furthermore, the interaction of fault slip and off-fault plasticity results in pockets of slip deficit. While the energy dissipated through plastic deformation remains a small fraction of the total energy budget, its impact on the source characteristics is disproportionally large through the redistribution of stresses and viscous relaxation. Our results suggest a new mechanism of dynamic heterogeneity in earthquake physics that may have important implications on earthquake size distribution and energy budget.

Plain Language Summary

Earthquakes are among nature's deadliest and costliest hazards. Physics-based simulations are essential to complement the lack of data and elucidating the complex patterns of earthquakes. This work discovers a new mechanism for regulating earthquake dynamics that emerges due to the interaction between fault slip and fault zone plasticity. It enables transition from periodic events to fully irregular sequences of earthquakes. The impact of plasticity on earthquake source characteristics goes beyond its limited contribution to the overall energy budget. Plasticity plays a crucial role in the redistribution of stresses which may inhibit earthquake growth and leads to clustering of seismicity. This work highlights the need for characterizing the fault zone mechanical response beyond their elastic properties to better inform seismic hazard models.

1. Introduction

Earthquakes are a prime example of a complex natural processes with far-from-equilibrium strongly nonlinear dynamics, having substantial societal and economic relevance for large populations worldwide. The lack of quantitative data on timescales capturing multiple large earthquake cycles is a long-standing challenge (Scharer & Yule, 2020; Bemis et al., 2021). Physics-based simulations provide a path to complement the lack of data and to elucidate multi-scale dynamics and spatio-temporal patterns that extend the knowledge beyond sporadic case studies and regional statistical laws (Barbot et al., 2012; Noda & Lapusta, 2013; Jiang & Lapusta, 2016).

Resolving wide range of spatio-temporal scales associated with earthquake nucleation, propagation, and arrest is a major challenge in modeling earthquakes (Shaw & Rice, 2000). Spatial scales may range from few milimeters of process zone near the rupture tip to several kilometers of fault length (Rice 2006). Temporal scales range from years of aseismic slip associated with tectonic loading to few seconds in co-seismic rapid rupture (Rice & Ben-Zion, 1996). Simulating a single rupture may not be sufficient to get insights into the full history of fault slip as it involves artificial nucleation and depends critically on the prescribed initial conditions (Ampureo & Ben-Zion, 2008). Modeling Sequence of Earthquake and Aseismic Slip (SEAS) bridges the spatio-temporal scales to illuminate pattern of earthquake cycles over long time as well as evolution of fault slip both during seismic ruptures and inter-seismic intervals (Lapusta et al., 2000; Lapusta & Liu, 2009; Abdelmeguid et al., 2019; Erickson et al., 2020; Jiang et al., 2021).

The majority of previous SEAS studies have been conducted either with fully elastic bulk or limited to the quasi-dynamic approximation where inertia effects, crucial for the dynamic phase, are not fully considered but only approximated through radiation damping (Rice 1993). Earthquake sequences for a planar fault with elastic bulk usually exhibit a periodic pattern (Lapusta et al., 2000). A mixture of large and small events may arise on planar faults in purely elastic bulk given sufficient quenched heterogeneity, e.g., variability in frictional properties (Lapusta & Rice, 2003; Kaneko et al., 2010) or incorporation of a compliant fault zone relative to the host rock (Abdelmeguid et al., 2019; Thakur et al. 2020) or if the fault is too long compared to the characteristic frictional-elastic length scale (Cattania, 2019; Barbot, 2019). A few studies have considered earthquake sequence simulations on non-planar faults (Dal Zilio et al., 2019; Sathiakumar et al., 2020) where a fault bend results in aperiodic seismicity with partial rupture. Cattania and Segall (2021) showed that within the quasidynamic approximation limit, non-planar faults having long wavelength fractal roughness may generate foreschocks and microseismicity. Tal et al. (2018) also studied the effect of fault roughness on earthquake nucleation using a fully dynamic simulation but assuming the bulk remain linear elastic.

Only a handful of studies investigated the effect of bulk material response, beyond elasticity, on sequence of earthquake and aseismic slip. These include quasi-dynamic cycle simulations with bulk viscoelasticity (Allison & Dunham, 2018, 2021), and the extension to the fully dynamic cycle simulation (Duru et al., 2019). Temperature dependent viscous flow has recently been considered and is shown to reduce the creeping of the velocity strengthening portion of the fault (Allison & Dunham, 2021). Using numerical simulations of single dynamic rupture events, it has long been recognized that off-fault plasticity acts as an energy sink and influences the rupture characteristics by reducing peak slip rate and limiting rupture speed (Templeton & Rice, 2008; Viesca et al., 2008; Dunham et al. 2011a, 2011b; Gabriel et al. 2013). Also, field observations identifying off-fault damage signifies the importance of non-linear bulk rheology, such as viscoplasticity, and its effects on long term seismicity pattern (Mitchell & Faulkner, 2009; Faulker et al., 2010; Lewis & Ben-zion, 2010; Liu & Hasterok, 2016). The effect of off-fault plasticity in cycle simulation has been investigated by Erickson et al. (2017). This study, however, was limited to the quasi-dynamic approximation and showed that the pattern of seismic cycle is like the reference elastic case except for slip deficit near free surface. It is not clear whether this insignificant difference between the plastic and elastic cases is intrinsic or is a consequence of the choice of the parameters and approximations involved. This is critical to investigate since natural fault zones exhibit significant inelastic response, which may be idealized as visco-plastic, and their evolution over short and long-time scales ought to be playing a role in the source physics.

Here, we investigate the effect of off-fault plasticity throughout the earthquake cycle while accounting for full inertia effect during the seismic phase using a hybrid finite element–spectral boundary integral scheme (Abdelmeguid et al., 2019). Using this technique, we explore the patterns of earthquake cycles as the off-fault bulk properties, namely the yield strength and viscous relaxation time scales, are varied. We outline the setup of the model and summarize the main results in the next sections.

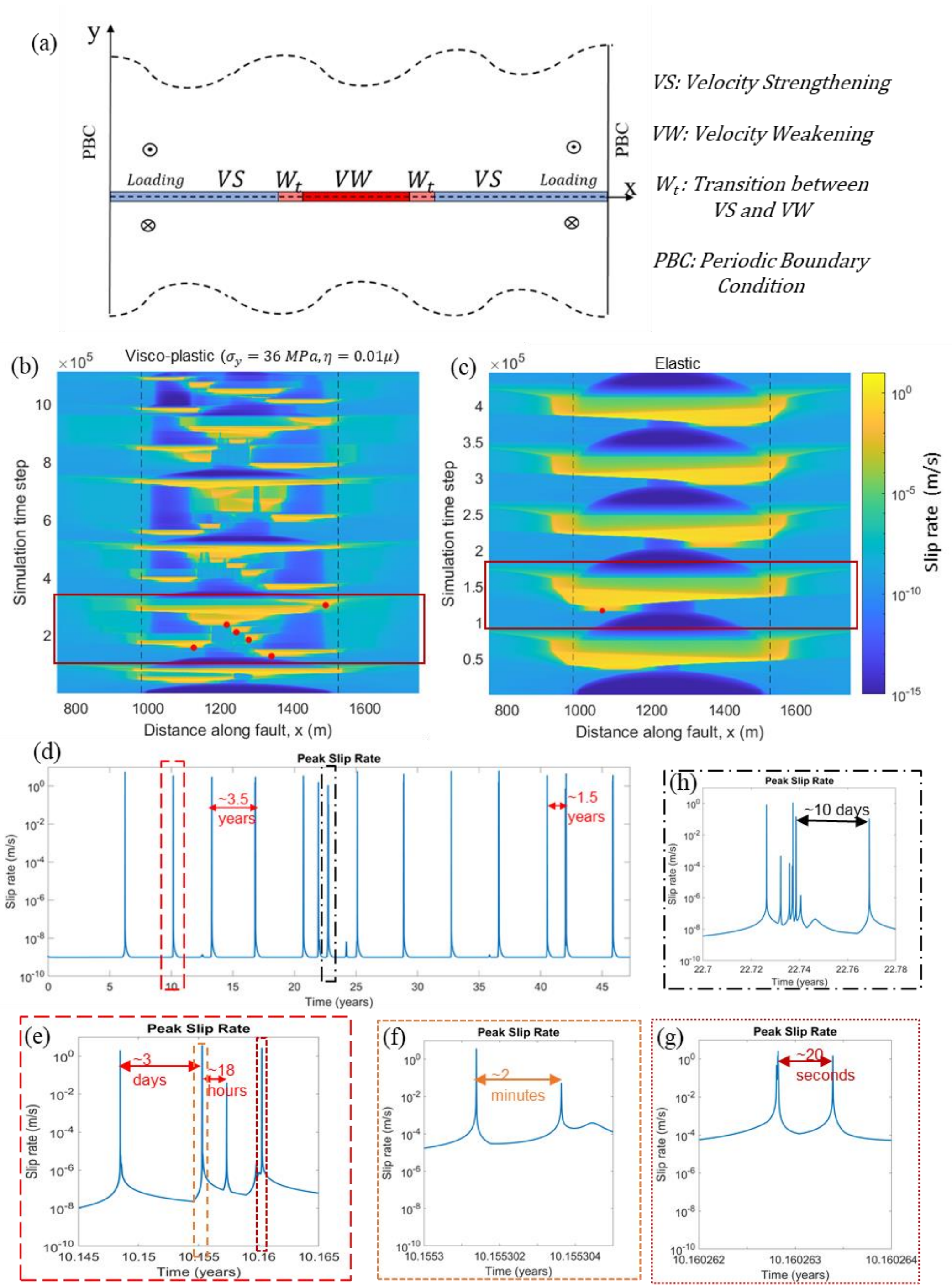

Figure 1. Sequence of earthquakes and aseismic slip on a 2D anti-plane rate-and-state fault (a) Model setup. (b) Slip rate evolution for viscoplastic case (yield strength, $\sigma_y = 36\ MPa$, viscosity, $\eta = 0.01\mu$) illustrating spatio-temporal clustering of sesmic events in contrast to the elastic reference (shown in c) with simple periodic cycles. Both (b) and (c) show results up to 25 years, and region in-between the vertical dashed lines is VW. Complexity persists beyond the time range shown here (Please see Supplementary Figure-S5). Red circles indicate nucleation sites of different events in cluster-2 (within the rectangular box). (d) history of peak slip rate showing aperiodic seismic cycles with time interval in the scale of years. (e, f, g) zoomed-in view for cluster-2 showing temporal clustering of seismic events with time interval spanning days to seconds. (h) zoomed-in view of cluster-7 showing existence of temporal clustering.

2. Model Setup and Methods

We consider a 2D anti-plane fault containing velocity-weakening (VW) and creeping velocity strengthening (VS) patches (Figure-1a). The fault is embedded in a full-space with no free surface. The length of the VW patch, $L_{VW} = 500\, m$ ($L_{VW} \approx 5\, L_{nuc}$), where L_{nuc} is the estimated nucleation size (Rubin & Ampuero, 2005). Out-of-plane loading is applied in the form of constant plate rate, $V_p = 35\, mm/year \approx 10^{-9} m/s$. The fault friction is governed by a regularized rate-and-state friction with state evolution following aging law (Dieterich, 1979; Ruina, 1983; Ben-Zion & Rice, 1997; Lapusta et al., 2000; Ampuero & Rubin, 2008). Off-fault material response is considered as elastic-viscoplastic. We consider J2 plasticity model with Perzyna viscoplastic relation (Perzyna, 1971; Simo & Hughes, 2006). As a limiting case to visco-plasticity (rate-dependent plasticity), we also simulate elastic-perfectly plastic (rate-independent plasticity) case. More details on model setup including list of parameters and distribution of frictional parameters used in the simulations are presented in Supplementary Information (Text-S1, Table-S1, Figure-S1).

To solve the governing field equations, we employ a hybrid finite element-spectral boundary integral scheme which fully accounts for inertial effects during episodes of rapid slip by alternating between a quasi-dynamics algorithm during the interseismic period, and a dynamics solver during seismic slip. Spectral boundary integral enables truncating the computational domain by replacing the exterior homogeneous linear elastic half spaces with integral relation between the shear stress and displacement history. The finite element discretization includes the fault and the near-field nonlinear bulk. More details about the methods are outlined in Supplementary Information (Text-S2, Figure-S2).

We simulate earthquake cycles for the model geometry shown in Figure-1a to investigate the implications of different off-fault bulk rheologies such as: elastic; elastic-viscoplastic; and elastic-perfectly plastic. To investigate factors affecting the off-fault material response, we also vary the yield strength and viscosity.

3. Results

3.1 Spatio-temporal Clustering of Seismicity

Figure-1 shows the evolution of slip rate with and without off-fault plasticity. With off-fault plasticity, seismic events are clustered in space and time with a mixture of partial ruptures and fault-spanning events (Figure-1b) whereas the elastic case generates simple periodic fault-spanning events (Figure-1c). During aseismic deformation, the active fault (VW region) remains almost locked demonstrated by the slip rate far below the loading ($V_p = 10^{-9} m/s$) whereas the velocity strengthening (VS) region keeps creeping following the loading. During rapid rupture, the VW region moves with increasing slip rate as the rupture propagates. The arrest of rupture is indicated by subsequent decrease in slip rate. For the elastic simulation (Figure-1c), all seismic events rupture the entire VW region and get arrested after reaching the VS region. On the other hand, for the plastic simulation (Figure-1b), not all events rupture the full length of the VW region. Rupture arrest is observed within VW region followed by nucleation of subsequent events highlighting the spatial migration and clustering. The red circles in Figure-1b mark the nucleation sites of different events in cluster-2. It shows that the nucleation site in this case does not necessarily exist near the end of VW region as observed in the elastic simulation (Figure- 1c). Rather the nucleation site jumps from one location to another during different events. That is, subsequent events nucleate within the VW region and not necessarily due to the expansion of creep fronts from the VS region as in Figure-1c. The rupture arrest is associated with plastic strain accumulation and the arrest of partial rupture leaves stress concentration which in turn affects the nucleation and rupture characteristics of subsequent events.

Furthermore, while the elastic case is characterized by simple periodic events, the elastic-visco-plastic case exhibits temporal clustering of seismicity. The time history of peak slip rate (Figure-1d) shows the aperiodic sequence of earthquake and aseismic slip that emerge with plasticity. Before and after the seismic event, the peak slip rate is close to the applied plate rate ($V_p = 10^{-9} m/s$) indicating aseismic slip. The occasional sharp increase of peak slip rate denotes the fast rupture of the velocity weakening zone during the seismic event which apparently looks like vertical lines (Figure-1d). If we zoom in the time scale as shown in Figure-1e-1h it reveals a richer structure spanning multiple time scales. Specifically, the apparent vertical lines in Figure-1d are temporal clusters of seismicity encompassing multiple subevents with interevent time spanning days to seconds whereas the interevent time of each cluster of events as shown in Figure-1d is in the scale of years (1.5-3.5 years). Within cluster-2, for example, there are in total 6 events (Figure-1e, 1f, 1g). The first two events occur within a few days apart (Figure-1e); the next event is found within next few minutes (Figure-1f). The last two events are found only in few seconds (Figure-1g). We compute the seismic moment and corresponding moment magnitude (M_w) of the events considering unit width of the fault plane. The largest magnitude is $M_w \approx 2$ (Supplementary Information, Figure-S6). Magnitudes of events in cluster-2 vary from $M_w = 0.5$ to $M_w = 1.8$. The temporal clustering prevails in subsequent clusters (Figure-1h) even though the interevent times and magnitudes may vary from one cluster to another. This Russian-doll-like temporal clustering of seismicity is qualitatively similar to natural seismicity (Ortega-Romo & Chen, 2021; Schurr et al., 2014; Konca et al., 2008) and suggest a crucial role of off-fault plasticity in modulating rupture growth and arrest.

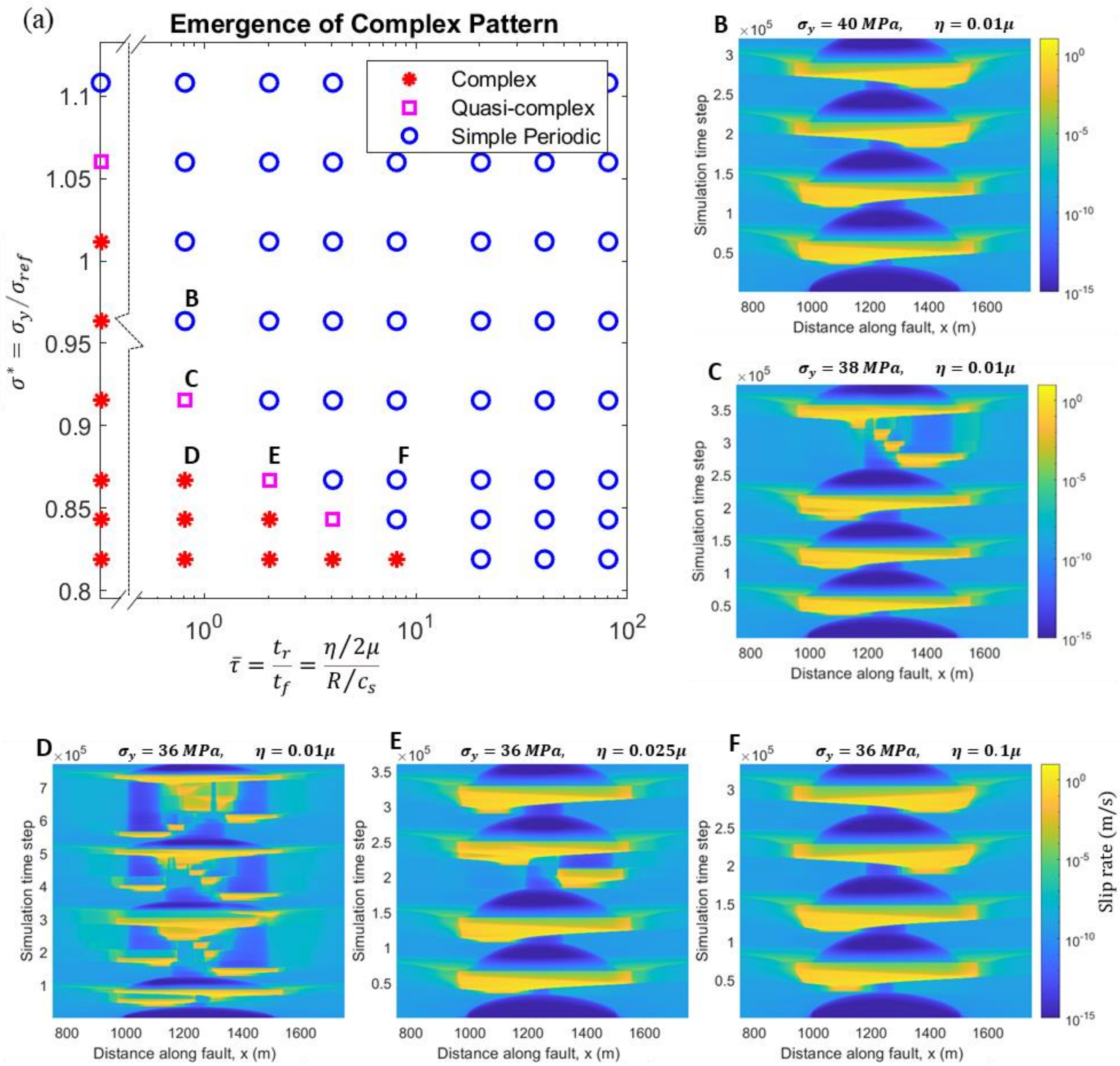

Figure 2. Emergence of complex seismic pattern depending on yield strength and viscosity. (a) Summary of seismicity patterns generated by varying yield strength and viscosity. Yield strength (σ_y) is normalized by a reference stress, $\sigma_{ref} = \sigma_n[f_0 + a\, ln(V_{seismic}/V_p)] \approx 41.5\ MPa$, which is an estimation of peak stress for elastic case accounting direct effect in rate-and-state friction. Relaxation time is normalized by time scale associated with frictional weakening within the process zone, $t_f = R/c_s = 0.0062\ s$. Complex patterns are found for lower yield strength and lower range of viscosity. For a particular viscosity, decrease in yield strength leads to transition from periodic to quasi-complex and complex pattern (as shown in **B**, **C**, and **D**). For a particular yield strength, decrease in viscosity leads to the emergence of spatiotemporal clustering as shown in **D**, **E,** and **F**. Rate independent plasticity also shows transition from periodic to complex pattern when yield strength is decreased.

3.2 Emergence of Complex Pattern

To explore the robustness of the spatiotemporal complexity, we have carried out several simulations by varying bulk yield strength and viscosity. The viscosity is varied over two orders of magnitude which corresponds to varying the relaxation time, $t_r = \eta/2\mu = 0.005 - 0.5\ s$. Estimates for viscosity, and consequently the relaxation time, of crustal rocks vary widely between $10^{18} - 10^{25}\ Pa - s$ (Liu & Hasterok, 2016; Allison & Dunham, 2018; Behr 2022) at strain rates lower than $10^{-13}s^{-1}$ to $10^{10}\ Pa - s$ at higher strain rates ($10^{-4}s^{-1}$) (Döhmann et al., 2019, Makhnenko & Podladchikov, 2018). Extrapolating to co-seismic strain rates ($10^{-2}s^{-1}$) would suggest even smaller viscosities and relaxation times of the order of $0.005\ s$. Furthermore, studies on rate sensitivity in rock strength and damage at co-seismic strain rates suggest that the response is weakly rate dependent (Olsson, 1989; Beeler et al., 2007; Yang et al., 2020) at least for strain rates up to $10^{0}s^{-1}$. This is also consistent with other studies which implemented Perzyna viscoplastic regularization during dynamic rupture simulations and used low values of viscosity (Dunham et al., 2011; Tal & Faulkner, 2022). Therefore, here we explore both the rate-independent and weakly rate dependent limits during the co-seismic periods and allow for a stronger viscous response at lower slip rates. Specifically, we assume a pseudo shear-rate thinning rheology (Weijermars, 1997) where we use adaptive relaxation during aseismic slow deformation (low strain rate) allowing viscosity to increase as the peak slip rate decreases while keeping the intended relaxation time fixed during coseismic deformation (high strain rate). The complexity in seismicity pattern is also found to be qualitatively similar when we use fixed relaxation time throughout aseismic and coseismic deformation. (Supplementary Information, Figure-S3). More experimental studies are required to better constrain the rate-dependent inelastic response of rocks under a variety of seismogenic conditions.

Different patterns of seismicity depending on yield strength and viscosity are summarized in Figure-2. We normalize bulk yield strength, σ_y, by a reference stress, $\sigma_{ref} = \sigma_n\left[f_0 + a\ ln\left(V_{seismic}/V_p\right)\right] \approx 41.5\ MPa$, which estimates peak stress at a rupture tip within the elastic bulk accounting for the direct effect in rate-and-state friction. Relaxation time is also normalized by a time scale associated with friction. Since the change in frictional stress occurs over the length of process zone, $R = \mu L/\sigma_n b = 21.36\ m$, we choose the time scale associated with frictional weakening within the process zone to be $t_f = R/c_s = 0.0062\ s$, where c_s is the shear wave speed. For a given yield strength, when viscosity is decreased, we observe transition in the pattern of seismicity from simple periodicity to spatio-temporal complexity through a quasi-complex pattern. For instance, with yield strength, $\sigma_y = 36\ MPa$ ($\sigma^* \approx 0.87$), simple periodic patterns of seismic cycles are found for viscosity exceeding 0.05μ ($\bar{\tau} \approx 4.05$) but complex pattern is observed when viscosity is reduced to 0.01μ ($\bar{\tau} \approx 0.81$). For intermediate viscosities, quasi-complex event sequences may emerge. We distinguish complex pattern by spatiotemporal clustering of seismic events prevailing in almost every cluster whereas quasi-complex pattern is nearly periodic with occasional emergence of partial ruptures. The transition to complexity with the reduction in the viscosity may be explained as follows. The redistribution of stresses occurs over two time scales: the viscous relaxation time scale and the time scale associated with frictional weakening within the process zone. At high viscosity, the relaxation time scale is long, and the stresses are redistributed rapidly over the time scale associated with frictional weakening within the process zone. This is similar to the elastic case. At low viscosity, the redistribution of stresses due to viscous relaxation is faster or as fast as the time scale associated with frictional weakeing within the process zone and thus complexity emerge due to the competition of these two processes.

However, the transition also depends on the yield strength. When yield strength is increased from $36\ MPa$ to $40\ MPa$ ($\sigma^* \approx 0.87\ to\ 0.96$) keeping the viscosity fixed such as $\eta = 0.01\mu$ ($\bar{\tau} \approx 0.81$), the seismic pattern becomes periodic through a quasi-complex pattern for the intermediate yield strength of $38\ MPa$ ($\sigma^* \approx 0.92$). This indicates that, for a particular viscosity, a decrease in yield strength, favoring higher accumulation of off-fault plasticity, gives rise to complex seismic pattern. In the limiting case of rate independent plasticity, complexity of earthquake sequences persists for all values of yield stress up to $\sigma^* \sim 1$ suggesting the critical role of off-fault plasticity in pinning the rupture tip and leading to spatio-temporal clustering of seismicity by limiting the ability of the crack to concentrate the stress beyond the yield limit as will be discussed shortly.

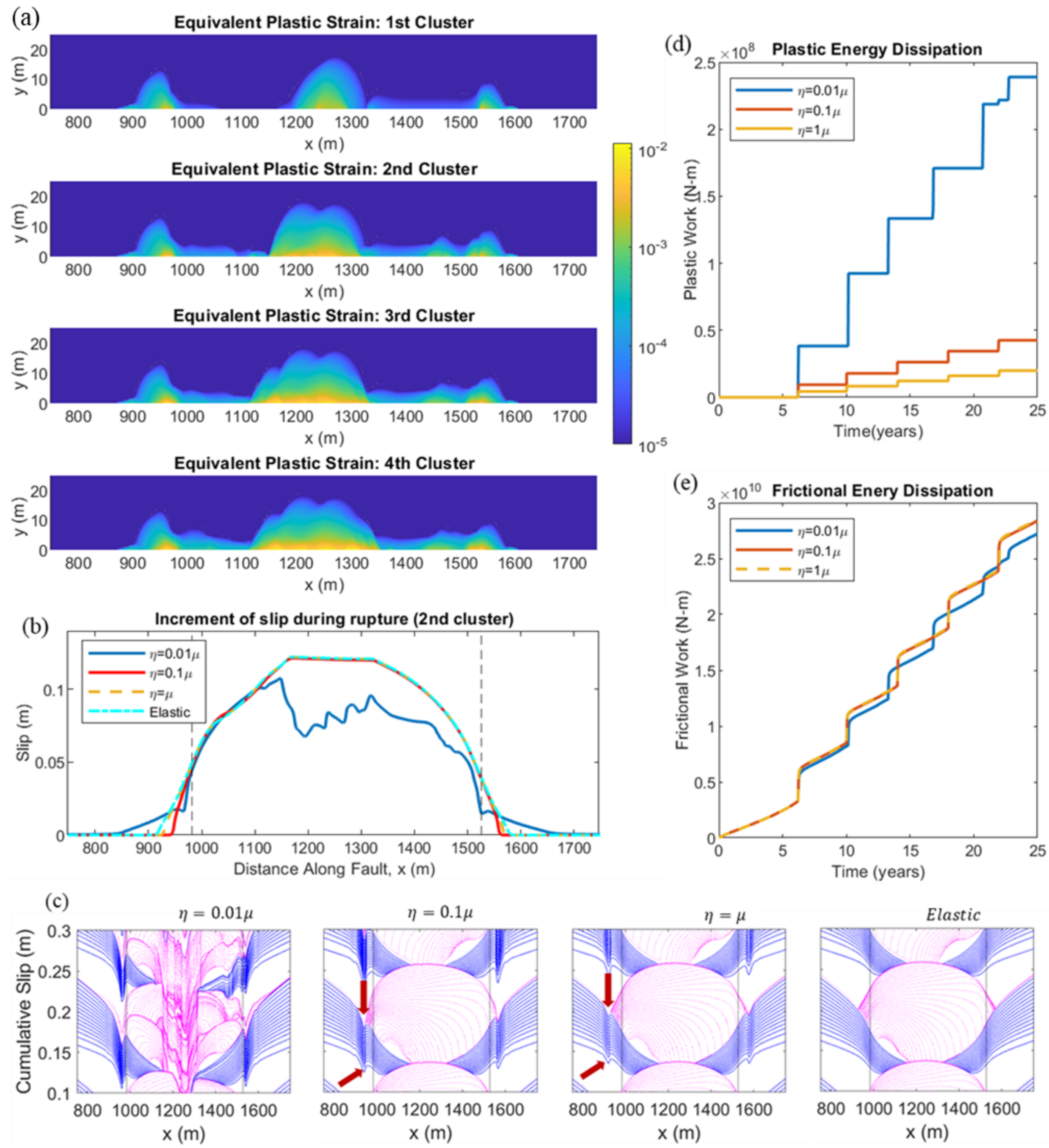

Figure 3. Evolution of plastic strain and effect of viscosity. (a) Spatial distribution of equivalent plastic strain after cluster of events (yield strength, $\sigma_y = 36\ MPa$, viscosity, $\eta = 0.01\mu$). Plastic strain accumulation spreads along the fault with successive cluster. (b) Increment of slip during rupture in the 2nd cluster. (c) Cumulative slip distribution where solid blue lines are plotted at every 3 months during aseismic slip and dotted magenta lines are at every 10 milliseconds during dynamic rupture. Lower viscosity case generates non-uniform slip while higher viscosity case is almost like elastic case except slip deficit near rupture arrest (as shown in b and c). (d) Evolution of plastic energy dissipation. (e) Evolution of frictional energy dissipation. Decrease in viscosity increases plastic dissipation but overall plastic dissipation is small compared to frictional dissipation (compare scales of d and e).

3.3 Evolution of off-fault plasticity and fault slip

A key contribution of this work is tracking the co-evolution of off-fault plastic strain with the accumulation of fault seismic and aseismic slip over long time scales. In Figure-3a spatial distribution of equivalent plastic strain shows that plasticity primarily contained within relatively narrow region normal to the fault while rest of the bulk remains elastic. We chose half-width of the FEM strip as 30 m ($\approx 1.5\ R$) which is found to contain the plastic zone. Spatial distribution of plastic strain is symmetric across the fault as there are no variations in the normal stress associated with slip in the 2D anti-plane problem. However, most notably, the accumulation of plastic strain is non-uniform along the fault. Plastic strain is higher in the region where rupture gets arrested. Multiple clusters of events lead to the non-uniform spreading of off-fault plastic strain parallel to the fault. Figure-3b shows the spatial distribution of slip accumulation within event cluster-2. The final slip distribution during this cluster shows that the VW region of the fault experienced extensive co-seismic sliding compared to the VS region. Basically, slip deficit created by the slow creeping of the VS regions during aseismic deformation is compensated by the sliding of VW region through coseismic rupture. Higher viscosity cases ($\eta = 0.1\mu,$ and $\eta = \mu$) show smooth distribution of slip like the elastic case except small deficit near the rupture arrest region as indicated by the arrows in Figure-3c. On the other hand, there are oscillations in the spatial distribution of slip with lower viscosity ($\eta = 0.01\mu$). Oscillations in the slip distribution arises from spatiotemporal clustering of seismic events with irregular nucleation, heterogenous propagation, and arrest of the rupture. For the low viscosity case, slip deficit is pervasive reflecting the significant partitioning of total deformation into fault slip and off-fault plastic deformation of the bulk.

Plastic dissipation increases as viscosity decreases (Figure-3d). When viscosity is reduced from $\eta = \mu\ to\ \eta = 0.1\mu$, the plastic dissipation increases. However, the increase in plastic dissipation is much higher when viscosity is reduced from $\eta = 0.1\mu$ to $\eta = 0.01\mu$. Nonetheless, overall plastic energy dissipation is found to be very small compared to the frictional energy dissipation (attention to the scales of Figure-3d, 3e). For instance, in cluster-2 for $\eta = 0.01\mu$, plastic dissipation is below 3% of the corresponding frictional dissipation whereas plastic dissipation is below 0.6% of the corresponding frictional dissipation for the case of $\eta = 0.1\mu$. In both higher and lower range of viscosity, plastic dissipation is smaller than frictional dissipation. While, the off-fault plastic dissipation remains small, plasticity, depending on the parameters, plays a crucial role in altering the pattern of earthquake sequences through its impact on stress redistribution and its heterogeneity. This effect is intensified as the viscosity and yield strength decrease.

Specifically, the emergence of complex spatio-temporal clustering of seismicity is attributed to the plastic strain accumulation and resulting stress heterogeneity but not necessarily the fraction of energy dissipated globally in plastic work. Off-fault plastic strain pins the crack motion through acting as an additional local energy sink, adding to the breakdown energy at the crack tip, and increasing the effective toughness of the medium. Furthermore, off-fault plasticity reduces the stress concentration ahead of the crack tip by limiting the stress to a smaller value than what could be achieved for an elastic bulk. This stress limiting effect increases as the viscosity decreases, and for the rate-independent limit the stress ahead of the crack tip does not exceed the yield stress. This reduction in the ability to concentrate the stress leads to the arrest of the seismic rupture even within the velocity weakening patch and to the frequent emergence of partial ruptures. In the purely elastic case, only fault spanning ruptures emerge and the rupture arrest takes place in the velocity strengthening patch. In the elastic case, as the rupture propagates, the stress increases ahead of the rupture front, and the stress concentration effect, as measured for example by a stress intensity factor, increases with rupture propagation. For the elastic-viscoplastic case, the stress may exceed the yield strength, depending on the loading rate and viscosity. The lower the viscosity is, the smaller this stress overshoot will be, and the more plastic strain will accumulate. Similarly, lower yield strength corresponds to higher plastic strain accumulation. This plastic response of the bulk introduces stress heterogeneity which affects rupture nucleation, propagation, and arrest. Figure-4 illustrates the state of stress close to the fault plane during coseismic rupture for the first event with elastic-perfectly plastic bulk ($\sigma_y = 36\ MPa, \sigma^* \approx 0.87$). Purely elastic bulk allows stress concentration ahead of the rupture tip which enables the rupture to propagate further. For elastoplastic bulk, however, off-fault plastic yielding limits the stress concentration which pins the crack tip and leads to rupture arrest. Furthermore, the jumping of the nucleation site that we reported in Figure-1b is a direct consequence of the generation of off-fault plastic strain ahead of the crack tip. As the rupture arrests and this plastic zone forms, the stress must increase on the fault beyond the plastic zone in order to nucleate a new event within an already stress relaxed region. As a result, the sequence of events appears segmented and the nucleation sites move from one location to another guided by the plastic strain distribution.

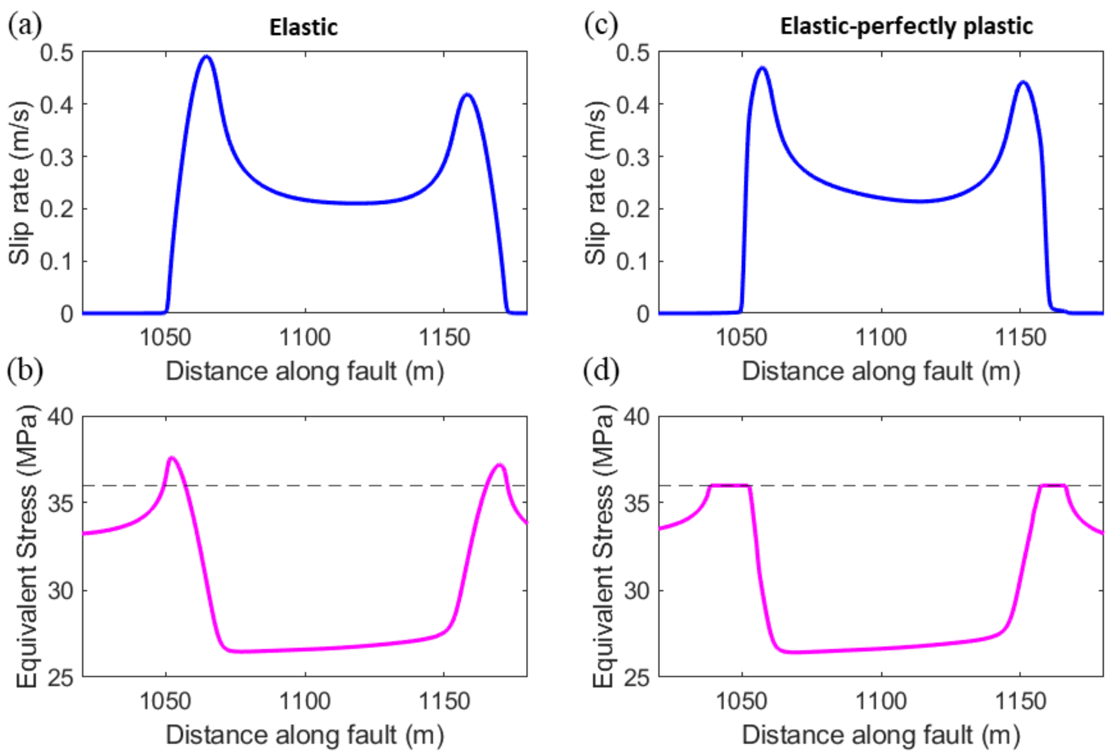

Figure 4. Comparison of the state of stress for elastic and elastic-perfectly plastic bulk. (a) and (b) respectively show spatial distribution of slip rate and equivalent stress ($\sqrt{\sigma_{xz}^2 + \sigma_{yz}^2}$) close to the fault plane for elastic case where stress concentration occurs ahead of the rupture tip. (c) and (d) correspond to elastic-perfectly plastic case (yield strength, $\sigma_y = 36\ MPa$). For elastic-perfectly plastic bulk, stress ahead of the rupture tip is bounded by the yield strength due to plastic yielding of the bulk. This reduced stress concentration with off-fault plasticity leads to rupture arrest. Horizontal dashed lines are drawn to mark the bulk yield strength.

4. Discussion

In this work, we showed how the co-evolution of fault slip and off-fault plasticity may lead to the emergence of spatio-temporal complexity of sequences of earthquakes and aseismic slip. This is a new mechanism for dynamic heterogeneity that has not been highlighted before and suggest the need for monitoring both on-fault and off-fault processes over multiple spatial and temporal scales as they are tightly coupled with strong feedback loops.

The hybrid numerical scheme combining finite element and spectral boundary integral enabled us to perform high resolution modeling of the complex nonlinear problem covering all phases of the seismic cycle from aseismic creep to fully inertial dynamic rupture while accounting for bulk plasticity. This enabled us to map the fault response over a wide range of parameters that were not accessible before. Our work suggests that two non-dimensional parameters control the transition from simple periodicity to spatio-temporal complexity; namely the ratio of the yield stress to the elastic peak stress and the ratio of the viscous relaxation time scale to the time scale associated with frictional weakening within the process zone. As viscosity decreases or the yield strength decreases, the off-fault plastic strain increases, and this coevolution of off-fault bulk plasticity and on-fault slip leads to clustering of seismicity in time and partial ruptures in space. The pinning effect of off-fault plasticity leads to rupture arrest and jumping of the nucleation site. This sheds light on a new mechanism for modulating the sequence of earthquake and aseismic slip.

Even though plastic dissipation is a small fraction of the total energy budget, its impact on the rupture dynamics is amplified by its feedback on stress heterogeneity. Global quantities like energy balance may not reveal the full picture of the source physics and there is a need for investigation of small-scale physics in complex fault zones due to their evolutionary nature and feedback loops they introduce. Besides, investigation with wider parameter space including variation in bulk yield strength and viscosity reveals the dependency of the pattern of seismic cycles on off-fault material properties like yield strength and viscosity. This indicates the need for accurately characterizing the nonlinear rheology of rocks.

Our model, even though with a relatively short fault ($L_{VW} \approx 5\ L_{nuc}$), exhibits complex seismicity pattern including partial rupture and temporal clustering. The complexity reported here does not require long faults (Cattania, 2019; Barbot, 2019) or rheological heterogeneity (Kaneko et al., 2010). Rather, it emerges naturally as a dynamic process due to the feedback between off-fault plasticity and on-fault stress heterogeneity which may occur at any scale. Specifically, off-fault plasticity may act as a self-limiting process for the growth of induced seismicity and hence may contribute to modulating seismicity at injection sites. This suggests that accounting for plasticity may be necessary even for small earthquakes and short faults.

A limitation of this study includes the lack of consideration of coseismic variation in elastic moduli as well as interseismic healing which has been widely documented and are suggested by some studies (Ben-Zion & Lyakhovsky, 2019; Ben-Zion & Huang, 2002; Tenthorey & Cox, 2006; Griffith et al., 2012). Furthermore, extending the model to 2D plane strain and full 3D may enrich the response through incorporation of normal stress changes and asymmetric generation of damage. Beyond the anti-plane setting, details of fault geometry such as non-planarity (Sathiakumar et al., 2020; Dal Zilio et al., 2019) or roughness (Cattania and Segall 2021; Tal & Faulkner, 2022) introduce stress heterogeneity which may influence off-fault plasticity and alter the seismicity pattern. Finally, different state evolution laws may affect aseismic plastic strain accumulation differently. We plan to incorporate these additional feedback mechanisms in future work.

Acknowledgement

The authors acknowledge support from the Southern California Earthquake Center through a collaborative agreement between NSF. Grant Number: EAR0529922 and USGS. Grant Number: 07HQAG0008 and the National Science Foundation CAREER award No. 1753249 for modeling complex fault zone structures. This material is also based upon work partially supported by the Department of Energy under Award Number DE-FE0031685 to investigate spatio-temporal complexity of induced earthquakes.

Data Availability Statement

The authors accept AGU's data policy. Data generated from numerical simulations are uploaded on repository and available online (https://doi.org/10.5281/zenodo.5799775).

References

Abdelmeguid, M., Ma, X., & Elbanna, A. (2019). A novel hybrid finite element-spectral boundary integral scheme for modeling earthquake cycles: Application to rate and state faults with low-velocity zones. *Journal of Geophysical Research: Solid Earth*, *124*(12), 12854-12881.

Albertini, G., Elbanna, A., & Kammer, D. S. (2021). A three-dimensional hybrid finite element--spectral boundary integral method for modeling earthquakes in complex unbounded domains. *International Journal for Numerical Methods in Engineering, 122, 6905-6923.*

Allison, K. L., & Dunham, E. M. (2021). Influence of Shear Heating and Thermomechanical Coupling on Earthquake Sequences and the Brittle-Ductile Transition. *Journal of Geophysical Research: Solid Earth*, *126*(6), e2020JB021394.

Allison, K. L., & Dunham, E. M. (2018). Earthquake cycle simulations with rate-and-state friction and power-law viscoelasticity. *Tectonophysics*, *733*, 232-256.

Ampuero, J. P., & Ben-Zion, Y. (2008). Cracks, pulses and macroscopic asymmetry of dynamic rupture on a bimaterial interface with velocity-weakening friction. *Geophysical Journal International*, *173*(2), 674-692.

Ampuero, J. P., & Rubin, A. M. (2008). Earthquake nucleation on rate and state faults–Aging and slip laws. *Journal of Geophysical Research: Solid Earth*, *113*(B1).

Barbot, S. (2019). Slow-slip, slow earthquakes, period-two cycles, full and partial ruptures, and deterministic chaos in a single asperity fault. *Tectonophysics*, *768*, 228171.

Barbot, S., Lapusta, N., & Avouac, J. P. (2012). Under the hood of the earthquake machine: Toward predictive modeling of the seismic cycle. *Science*, *336*(6082), 707-710.

Beeler, N. M., Tullis, T. E., Kronenberg, A. K., & Reinen, L. A. (2007). The instantaneous rate dependence in low temperature laboratory rock friction and rock deformation experiments. *Journal of Geophysical Research: Solid Earth*, *112*(B7).

Behr, W. M., Holt, A. F., Becker, T. W., & Faccenna, C. (2022). The effects of plate interface rheology on subduction kinematics and dynamics. *Geophysical Journal International*.

Bemis, S. P., Scharer, K., & Dolan, J. F. (2021). The San Andreas Fault paleoseismic record at Elizabeth Lake: Why are there fewer surface-rupturing earthquakes on the Mojave section?. *Bulletin of the Seismological Society of America*, *111*(3), 1590-1613.

Ben-Zion, Y., & Lyakhovsky, V. (2019). Representation of seismic sources sustaining changes of elastic moduli. *Geophysical Journal International*, *217*(1), 135-139.

Ben-Zion, Y., & Huang, Y. (2002). Dynamic rupture on an interface between a compliant fault zone layer and a stiffer surrounding solid. *Journal of Geophysical Research: Solid Earth*, *107*(B2), ESE-6.

Ben-Zion, Y., & Rice, J. R. (1997). Dynamic simulations of slip on a smooth fault in an elastic solid. *Journal of Geophysical Research: Solid Earth*, *102*(B8), 17771-17784.

Cattania, C., & Segall, P. (2021). Precursory slow slip and foreshocks on rough faults. *Journal of Geophysical Research: Solid Earth*, *126*(4), e2020JB020430.

Cattania, C. (2019). Complex earthquake sequences on simple faults. *Geophysical Research Letters*, *46*(17-18), 10384-10393.

Courant, R., Friedrichs, K., & Lewy, H. (1928). Über die partiellen Differenzengleichungen der mathematischen Physik. *Mathematische annalen*, *100*(1), 32-74.

Dal Zilio, L., van Dinther, Y., Gerya, T., & Avouac, J. P. (2019). Bimodal seismicity in the Himalaya controlled by fault friction and geometry. *Nature communications*, *10*(1), 1-11.

Dieterich, J. H. (1979). Modeling of rock friction: 1. Experimental results and constitutive equations. *Journal of Geophysical Research: Solid Earth*, *84*(B5), 2161-2168.

Döhmann, M. J. E. A., Brune, S., Nardini, L., Rybacki, E., & Dresen, G. (2019). Strain localization and weakening processes in viscously deforming rocks: Numerical modeling based on laboratory torsion experiments. *Journal of Geophysical Research: Solid Earth, 124*(1), 1120-1137.

Duru, K., Allison, K. L., Rivet, M., & Dunham, E. M. (2019). Dynamic rupture and earthquake sequence simulations using the wave equation in second-order form. *Geophysical Journal International*, *219*(2), 796-815.

Dunham, E. M., Belanger, D., Cong, L., & Kozdon, J. E. (2011). Earthquake ruptures with strongly rate-weakening friction and off-fault plasticity, Part 1: Planar faults. *Bulletin of the Seismological Society of America*, *101*(5), 2296-2307.

Dunham, E. M., Belanger, D., Cong, L., & Kozdon, J. E. (2011). Earthquake ruptures with strongly rate-weakening friction and off-fault plasticity, Part 2: Nonplanar faults. *Bulletin of the Seismological Society of America*, *101*(5), 2308-2322.

Erickson, B. A., Dunham, E. M., & Khosravifar, A. (2017). A finite difference method for off-fault plasticity throughout the earthquake cycle. *Journal of the Mechanics and Physics of Solids*, *109*, 50-77.

Erickson, B. A., Jiang, J., Barall, M., Lapusta, N., Dunham, E. M., Harris, R., ... & Wei, M. (2020). Community Code Verification Exercise for Simulating Sequences of Earthquakes and Aseismic Slip (SEAS). *Seismological Research Letters*, *91*(2A), 874-890.

Faulkner, D. R., Jackson, C. A. L., Lunn, R. J., Schlische, R. W., Shipton, Z. K., Wibberley, C. A. J., & Withjack, M. O. (2010). A review of recent developments concerning the structure, mechanics and fluid flow properties of fault zones. *Journal of Structural Geology*, *32*(11), 1557-1575.

Gabriel, A. A., Ampuero, J. P., Dalguer, L. A., & Mai, P. M. (2013). Source properties of dynamic rupture pulses with off-fault plasticity. *Journal of Geophysical Research: Solid Earth*, *118*(8), 4117-4126.

Griffith, W. A., Mitchell, T. M., Renner, J., & Di Toro, G. (2012). Coseismic damage and softening of fault rocks at seismogenic depths. *Earth and Planetary Science Letters*, *353*, 219-230.

Hajarolasvadi, S., & Elbanna, A. E. (2017). A new hybrid numerical scheme for modelling elastodynamics in unbounded media with near-source heterogeneities. *Geophysical Journal International*, *211*(2), 851-864.

Jiang, J., & Lapusta, N. (2016). Deeper penetration of large earthquakes on seismically quiescent faults. *Science*, *352*(6291), 1293-1297.

Jiang, J., Erickson, B. A., Lambert, V. R., Ampuero, J. P., Ando, R., Barbot, S. D., ... & van Dinther, Y. (2021). Community-driven code comparisons for three-dimensional dynamic modeling of sequences of earthquakes and aseismic slip (seas).

Kaneko, Y., Avouac, J. P., & Lapusta, N. (2010). Towards inferring earthquake patterns from geodetic observations of interseismic coupling. *Nature Geoscience*, *3*(5), 363-369.

Konca, A. O., Avouac, J. P., Sladen, A., Meltzner, A. J., Sieh, K., Fang, P., ... & Helmberger, D. V. (2008). Partial rupture of a locked patch of the Sumatra megathrust during the 2007 earthquake sequence. *Nature*, *456*(7222), 631-635.

Lapusta, N., Rice, J. R., Ben-Zion, Y., & Zheng, G. (2000). Elastodynamic analysis for slow tectonic loading with spontaneous rupture episodes on faults with rate-and state-dependent friction. *Journal of Geophysical Research: Solid Earth*, *105*(B10), 23765-23789.

Lapusta, N., & Rice, J. R. (2003). Nucleation and early seismic propagation of small and large events in a crustal earthquake model. *Journal of Geophysical Research: Solid Earth*, *108*(B4).

Lapusta, N., & Liu, Y. (2009). Three-dimensional boundary integral modeling of spontaneous earthquake sequences and aseismic slip. *Journal of Geophysical Research: Solid Earth*, *114*(B9).

Li, Q., Liu, M., & Zhang, H. (2009). A 3-D viscoelastoplastic model for simulating long-term slip on non-planar faults. *Geophysical Journal International*, *176*(1), 293-306.

Liu, L., & Hasterok, D. (2016). High-resolution lithosphere viscosity and dynamics revealed by magnetotelluric imaging. *Science*, *353*(6307), 1515-1519.

Lewis, M. A., & Ben-Zion, Y. (2010). Diversity of fault zone damage and trapping structures in the Parkfield section of the San Andreas Fault from comprehensive analysis of near fault seismograms. *Geophysical Journal International*, *183*(3), 1579-1595.

Ma, X., Hajarolasvadi, S., Albertini, G., Kammer, D. S., & Elbanna, A. E. (2019). A hybrid finite element-spectral boundary integral approach: Applications to dynamic rupture modeling in unbounded domains. *International Journal for Numerical and Analytical Methods in Geomechanics*, *43*(1), 317-338.

Ma, X., & Elbanna, A. (2019). Dynamic rupture propagation on fault planes with explicit representation of short branches. *Earth and Planetary Science Letters*, *523*, 115702.

Makhnenko, R. Y., & Podladchikov, Y. Y. (2018). Experimental poroviscoelasticity of common sedimentary rocks. *Journal of Geophysical Research: Solid Earth*, *123*(9), 7586-7603.

Mitchell, T. M., & Faulkner, D. R. (2009). The nature and origin of off-fault damage surrounding strike-slip fault zones with a wide range of displacements: A field study from the Atacama fault system, northern Chile. *Journal of Structural Geology*, *31*(8), 802-816.

Moczo, P., Robertsson, J. O., & Eisner, L. (2007). The finite-difference time-domain method for modeling of seismic wave propagation. *Advances in geophysics*, *48*, 421-516.

Noda, H., & Lapusta, N. (2013). Stable creeping fault segments can become destructive as a result of dynamic weakening. *Nature*, *493*(7433), 518-521.

Ortega-Romo, A. D., & Chen, X. (2021). Spatiotemporal Clustering of Seismicity During the 2018 Kilauea Volcanic Eruption. *Geophysical Research Letters*, *48*(8), e2020GL090859.

Olsson, W. A. (1989). *The effect of strain rate on the compressive strength of dry and saturated tuff* (No. SAND-89-1196). Sandia National Lab. (SNL-NM), Albuquerque, NM (United States).

Perzyna, P. (1971). Thermodynamic theory of viscoplasticity. *Advances in applied mechanics*, *11*, 313-354.

Rice, J. R. (2006). Heating and weakening of faults during earthquake slip. *Journal of Geophysical Research: Solid Earth*, *111*(B5).

Rice, J. R. (1993). Spatio-temporal complexity of slip on a fault. *Journal of Geophysical Research: Solid Earth*, *98*(B6), 9885-9907.

Rice, J. R., & Ben-Zion, Y. (1996). Slip complexity in earthquake fault models. *Proceedings of the National Academy of Sciences*, *93*(9), 3811-3818.

Rubin, A. M., & Ampuero, J. P. (2005). Earthquake nucleation on (aging) rate and state faults. *Journal of Geophysical Research: Solid Earth*, *110*(B11), 94-144.

Ruina, A. (1983). Slip instability and state variable friction laws. *Journal of Geophysical Research: Solid Earth*, *88*(B12), 10359-10370.

Sathiakumar, S., Barbot, S., & Hubbard, J. (2020). Earthquake cycles in fault-bend folds. *Journal of Geophysical Research: Solid Earth*, *125*(8), e2019JB018557.

Shaw, B. E., & Rice, J. R. (2000). Existence of continuum complexity in the elastodynamics of repeated fault ruptures. *Journal of Geophysical Research: Solid Earth*, *105*(B10), 23791-23810.

Schurr, B., Asch, G., Hainzl, S., Bedford, J., Hoechner, A., Palo, M., ... & Vilotte, J. P. (2014). Gradual unlocking of plate boundary controlled initiation of the 2014 Iquique earthquake. *Nature*, *512*(7514), 299-302.

Scharer, K. M., & Yule, D. (2020). A maximum rupture model for the southern San Andreas and San Jacinto faults, California, derived from paleoseismic earthquake ages: Observations and limitations. *Geophysical Research Letters*, *47*(15), e2020GL088532.

Simo, J. C., & Hughes, T. J. (2006). *Computational inelasticity* (Vol. 7). Springer Science & Business Media.

Tal, Y., Hager, B. H., & Ampuero, J. P. (2018). The effects of fault roughness on the earthquake nucleation process. *Journal of Geophysical Research: Solid Earth*, *123*(1), 437-456.

Tal, Y., & Faulkner, D. (2022). The effect of fault roughness and earthquake ruptures on the evolution and scaling of fault damage zones. *Journal of Geophysical Research: Solid Earth*, *127*(1), e2021JB023352.

Templeton, E. L., & Rice, J. R. (2008). Off-fault plasticity and earthquake rupture dynamics: 1. Dry materials or neglect of fluid pressure changes. *Journal of Geophysical Research: Solid Earth*, *113*(B9).

Tenthorey, E., & Cox, S. F. (2006). Cohesive strengthening of fault zones during the interseismic period: An experimental study. *Journal of Geophysical Research: Solid Earth*, *111*(B9).

Thakur, P., Huang, Y., & Kaneko, Y. (2020). Effects of low-velocity fault damage zones on long-term earthquake behaviors on mature strike-slip faults. *Journal of Geophysical Research: Solid Earth*, *125*(8), e2020JB019587.

Viesca, R. C., Templeton, E. L., & Rice, J. R. (2008). Off-fault plasticity and earthquake rupture dynamics: 2. Effects of fluid saturation. *Journal of Geophysical Research: Solid Earth*, *113*(B9).

Weijermars, R. (1997). *Principles of rock mechanics*. Alboran Science Publishing.

Yang, L., Wang, G., Zhao, G. F., & Shen, L. (2020). A rate-and pressure-dependent damage-plasticity constitutive model for rock. *International Journal of Rock Mechanics and Mining Sciences*, *133*, 104394.

Geophysical Research Letters

Supporting Information for

Spatio-Temporal Clustering of Seismicity Enabled by Off-Fault Plasticity

Md Shumon Mia[1,2], Mohamed Abdelmeguid[2], Ahmed E. Elbanna[2,3]

[1]Department of Mechanical Science and Engineering, University of Illinois at Urbana-Champaign, Urbana, IL, USA.

[2]Department of Civil and Environmental Engineering, University of Illinois at Urbana-Champaign, Urbana, IL, USA.

[3]Beckman Institute of Advanced Science and Technology, University of Illinois at Urbana-Champaign, Urbana, IL, USA.

Corresponding author: Md Shumon Mia (mmia2@illinois.edu)

Contents of this file

Introduction

The Supplementary Information includes:

- Text S1 provide details for the model setup including friction law and viscoplastic constitutive relation.
- Text S2 outlines the numerical methods.
- Table S1 contains list of parameters used in the simulations.
- Figure S1 shows distribution of rate-and-state friction parameters.
- Figure S2 shows the schematics of the set-up for hybrid finite element-spectral boundary integral scheme.
- Figure S3 shows results for fixed relaxation time which is qualitatively similar to corresponding adaptive relaxation case presented in the main text.

- Figure S4 shows results for fully quasi-dynamics case which is qualitatively similar to the fully-dynamics case.
- Figure S5 shows partial rupture as well as occasional rupture spanning entire VW region persist throughout the simulation time. Same plot with results up to 25 years are shown in main text Figure-1b.
- Figure S6 shows seismic moment and magnitude of events for yield strength, $\sigma_y = 36\ MPa$, viscosity, $\eta = 0.01\mu$.

Text S1. Model Setup

The fault friction is governed by a regularized rate-and-state friction (Dieterich, 1979; Ruina, 1983; Ben-Zion & Rice, 1997; Lapusta et al., 2000) where the friction coefficient, f, is a function of slip rate and state variable:

$$f(V, \theta) = asinh^{-1}\left[\frac{V}{2V_0} exp\left(\frac{f_0 + bln(V_0\theta/L)}{a}\right)\right]. \quad \text{(Eqn-1)}$$

Here, a and b are nondimensional frictional parameters related to direct effect and state evolution respectively. $a - b < 0$ indicates velocity weakening friction whereas $a - b > 0$ indicates velocity strengthening friction. L is critical slip weakening distance and θ is state variable which evolves following a prescribed aging law (Ruina, 1983; Ampuero & Rubin, 2008):

$$\frac{d\theta}{dt} = 1 - \frac{V\theta}{L} \ . \quad \text{(Eqn-2)}$$

We consider constant effective normal stress, σ_n. The fault strength is then expressed as $\sigma_n\, f(V, \theta)$. Off-fault bulk constitutive response is elastic-viscoplastic. We consider J2 plasticity model with viscous regularization. For 2D anti-plane problem, it reduces to a yield function:

$$F(\sigma) = \sqrt{(\sigma_{xz}^2 + \sigma_{yz}^2)} - \sigma_y \ . \quad \text{(Eqn-3)}$$

Where, σ_y is the bulk yield strength. With Perzyna type viscoplastic relation (Simo & Hughes, 2006), viscoplastic strain rate is expressed as,

$$\dot{\epsilon}_{xz}{}^{vp} = \gamma \frac{\partial F}{\partial \sigma_{xz}} \ , \ \text{and} \quad \dot{\epsilon}_{yz}{}^{vp} = \gamma \frac{\partial F}{\partial \sigma_{yz}} \quad \text{(Eqn-4a, 4b)}$$

$$\text{with } \gamma = \frac{\langle F(\sigma) \rangle}{\eta} \quad \text{(Eqn-5)}$$

where, η denotes viscosity. Bulk constitutive relation for the 2D anti-plane problem, assuming an additive decomposition of the strain, then follows:

$$\sigma_{xz} = 2\mu\,(\epsilon_{xz} - \epsilon_{xz}{}^{vp}), \ \text{and} \quad \sigma_{yz} = 2\mu\,(\epsilon_{yz} - \epsilon_{yz}{}^{vp}) \quad \text{(Eqn-6a, 6b)}$$

where, μ is the shear modulus and ϵ_{ij} indicates total strain.

Text S2. Methods

We use an alternating quasi-dynamics and fully inertial dynamics approach to capture full time history of the earthquake sequence including both slow aseismic creep and fast dynamic rupture. Quasi-dynamics approach approximate inertia through radiation damping whereas dynamics approach fully accounts inertia. The switching between the two solvers is enabled based on a threshold slip rate of $0.01\, m/s$ below which radiation damping contribution ($\mu V/2c_s$) is very small($\sim$0.1% of the quasi-static shear stress with elastic bulk). During aseismic slow deformation, we solve a series of static equilibria to get fault traction for a given slip constraint. Then radiation damping is used while satisfying fault boundary condition. Quasi-dynamics approach involves adaptive time increment based on slip rate (Lapusta et al., 2000; Abdelmeguid et al., 2019). On the other hand, explicit dynamics approach fully accounts for inertia effects and integrates the equations of motion with fixed time increment governed by Courant-Friedrichs-Lewy (CFL) condition (Courant et al., 1928). In the dynamics formulation, we use traction-at-split-node (TSN) to compute fault traction as function of slip rate (Moczo et al, 2007; Setare & Elbanna, 2017).

In spatial discretization, we employ a hybrid scheme (Albertini et al., 2021, Abdelmeguid et al., 2019) combining finite element and spectral boundary integral. A narrow strip containing the fault and potential elastoplastic bulk is discretized with finite element (FEM) and the rest of the homogeneous linear elastic half-spaces are replaced by spectral boundary integral equations (SBI). A sketch of the hybrid scheme set-up is shown in Supplementary Information (Figure S2). This hybrid scheme truncated the computational domain significantly and provide an exact transparent boundary condition for wave propagation. We use a mesh size ($dx = dy = 0.5\ m$) such that the characteristic length scale defined by the static estimate of the process zone size, $R = \frac{\mu L}{\sigma_n b} = 21.36\ m$ is resolved by around 40 elements. Width of the virtual strip is chosen so that any possible plastic strain generation is fully contained within the strip and SBI represents rest of the elastic bulk. Process zone size may give an estimate for the potential plastic zone across the fault (Templeton & Rice 2008) which may also depend on the choice of parameters and geometry. We chose half-width of the virtual strip as $30\ m$ ($\approx 1.5\ R$) which is found to contain the plastic zone. We use radial return algorithm with viscous regularization (Simo & Hughes, 2006) to update the stresses. During coseismic phase, time increment is smaller than relaxation time by at least one order of magnitude which makes the relaxation time scale well resolved by simulation time increment. During aseismic slow deformation, we adopt relaxation time following the simulation time increment so that relaxation time is sufficiently resolved by the simulation time increment. Results do not qualitatively change when we use fixed relaxation time throughout (Figure-S3). Besides, we carry out fully quasi-dynamic simulation and find the complex seismicity pattern. This suggests that complex seismicity pattern is not an artifact associated with switching between solvers (Figure-S4).

Computational savings associated with the hybrid finite element-spectral boundary integral scheme results from the truncation of computational domain. FEM discretization handles near fault complexities including material non-linearities and SBI enables replacing rest of the homogeneous linear elastic half space. Modelling the same problem only in FEM would require much wider domain in order to avoid wave reflection from the boundary (Ma et al., 2019; Ma & Elbanna 2019; Abdelmeguid et al., 2019; Albertini et al., 2021).

Computational time associated with SBI is comparable to the computational time associated with only one layer of finite elements at the truncating boundary (Albertini et al., 2021). Therefore, truncated computational domain in hybrid scheme reduces both computational time and memory requirements.

Table S1. List of parameters used in the simulations

Parameter	Symbol	Values
Effective normal stress on fault	σ_n	$50\ MPa$
Critical slip distance	L	$500 \times 10^{-6}\ m$
Plate rate	V_p	$10^{-9}\ m/s$
Reference Slip rate	V_0	$10^{-6}\ m/s$
Initial slip rate	V_{init}	$10^{-9}\ m/s$
Reference friction coefficient	f_0	0.6
Shear wave speed	c_s	$3464\ m/s$
Shear modulus	μ	$32.038\ GPa$
Yield strength	σ_y	$Variable$
Viscosity	η	$Variable$

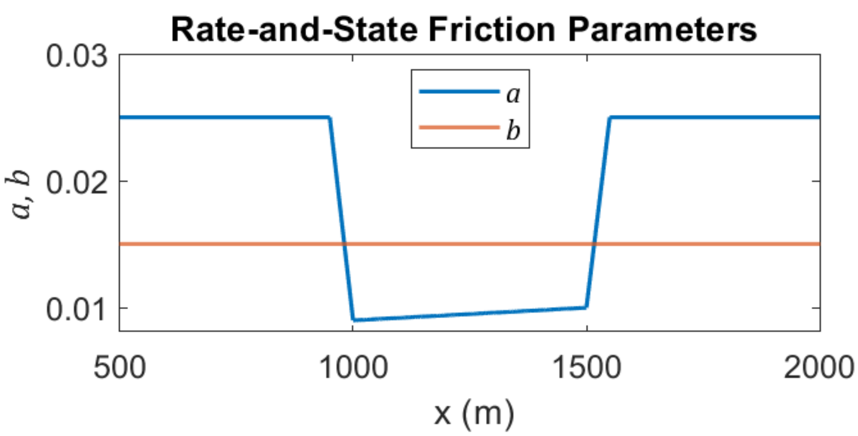

Figure S1. Distribution of rate-and-state frictional parameters. $\boldsymbol{a}$ and $\boldsymbol{b}$ are non-negative dimensionless rate-and-state frictional parameters related to direct effect and state evolution respectively. Velocity weakening (VW) patch is associated with $\boldsymbol{a} < \boldsymbol{b}$ and velocity strengthening (VS) refers to $\boldsymbol{a} > \boldsymbol{b}$.

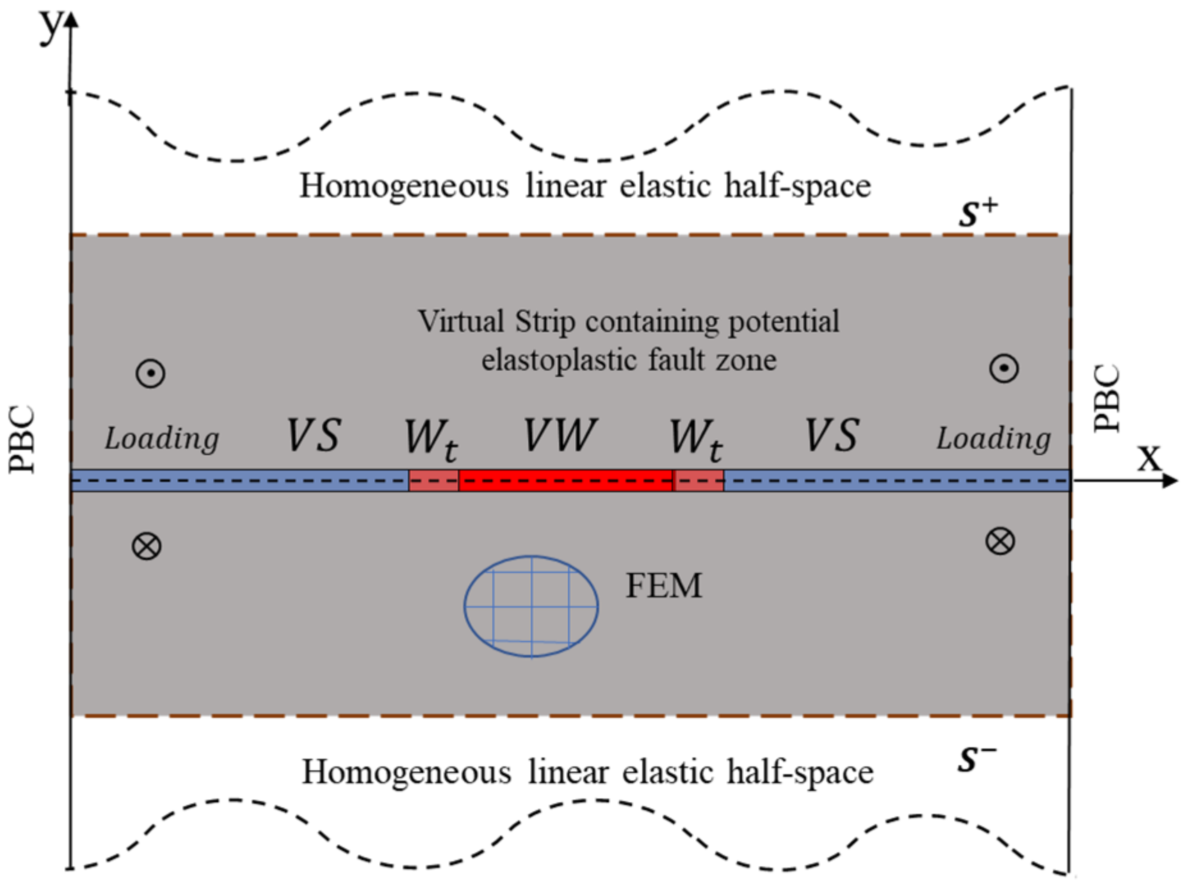

Figure S2. Hybrid scheme set-up. Narrow virtual strip containing fault and potential elastoplastic bulk is discretized with FEM. Spectral Boundary Integral (SBI) replaces homogeneous linear elastic half spaces at the virtual boundaries (S^+ and S^-). Periodic Boundary Conditions (PBC) are applied at the lateral boundaries.

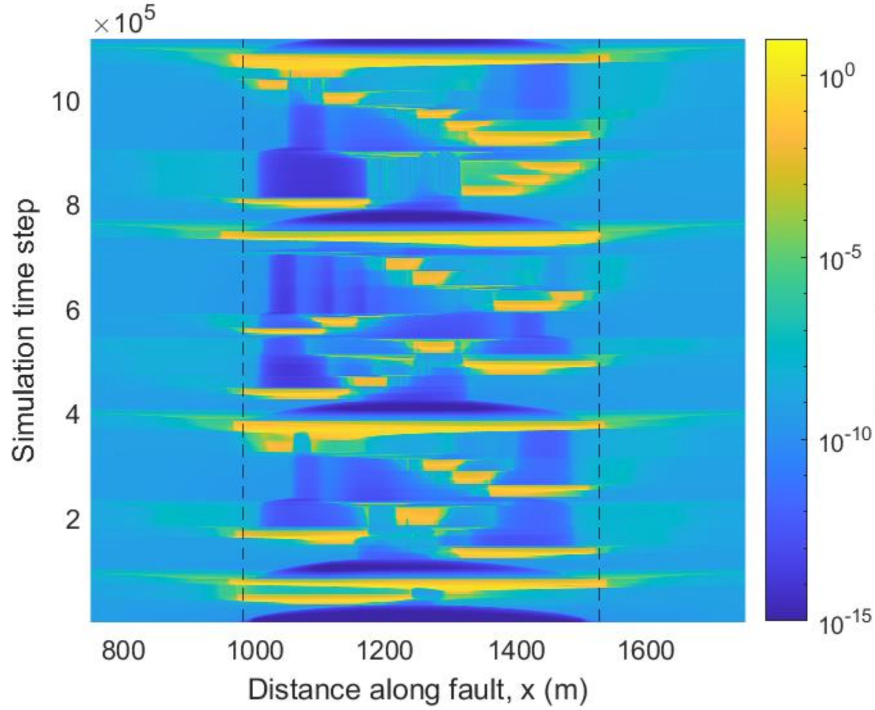

Figure S3. Spatio-temporal distribution of slip rate for fully-dynamics simulation with fixed relaxation (yield strength, $\sigma_y = 36\ MPa$, viscosity, $\eta\ = 0.01\mu$). Temporal clustering and partial rupture are observed which are qualitatively similar to the case with adaptive relaxation (Figure-1b in main text). Adaptive relaxation ensures that relaxation time scale is well resolved both in dynamics and quasi-dynamics phases assuming a shear thinning rheology where viscosity is varied during quasi-dynamics depending on peak slip rate and keeping the intended viscosity constant during dynamics. The features of complex seismicity pattern are qualitatively similar in both cases.

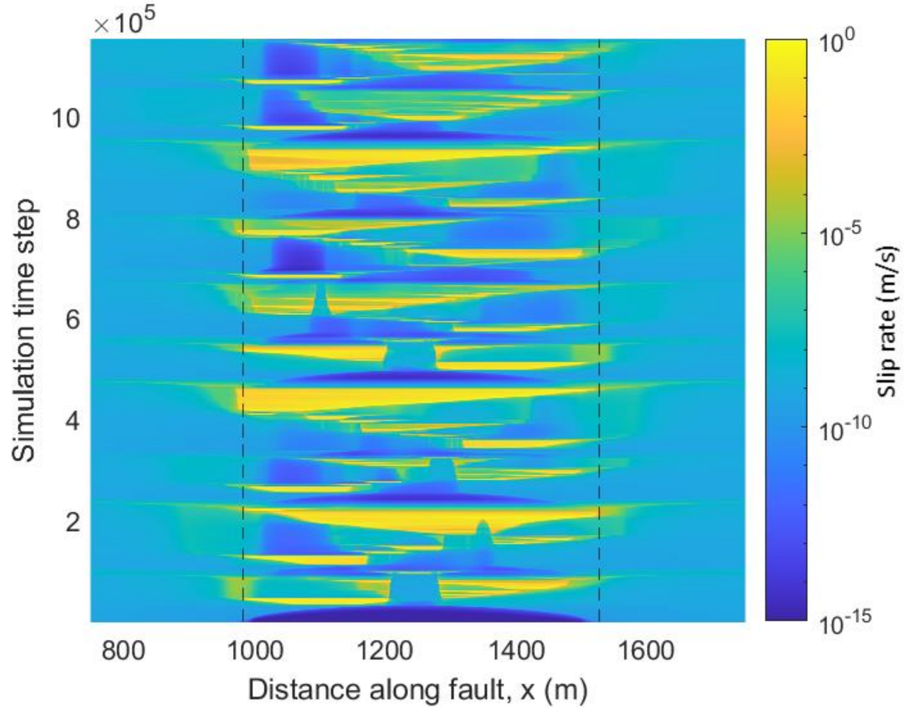

Figure S4. Spatio-temporal distribution of slip rate for quasi-dynamics simulation with adaptive relaxation (yield strength, $\sigma_y = 36\ MPa$, viscosity, $\eta\ = 0.01\mu$) where inertia is approximated with radiation damping. Features of complex seismicity pattern including temporal clustering and partial rupture are observed which are qualitatively similar to fully-dynamics simulation. Unlike fully-dynamics simulation, there is no switching between two alternating solvers in case of fully quasi-dynamics simulation. Therefore, these qualitatively similar results suggest that the complex seismicity pattern is not a possible artifact of switching between solvers.

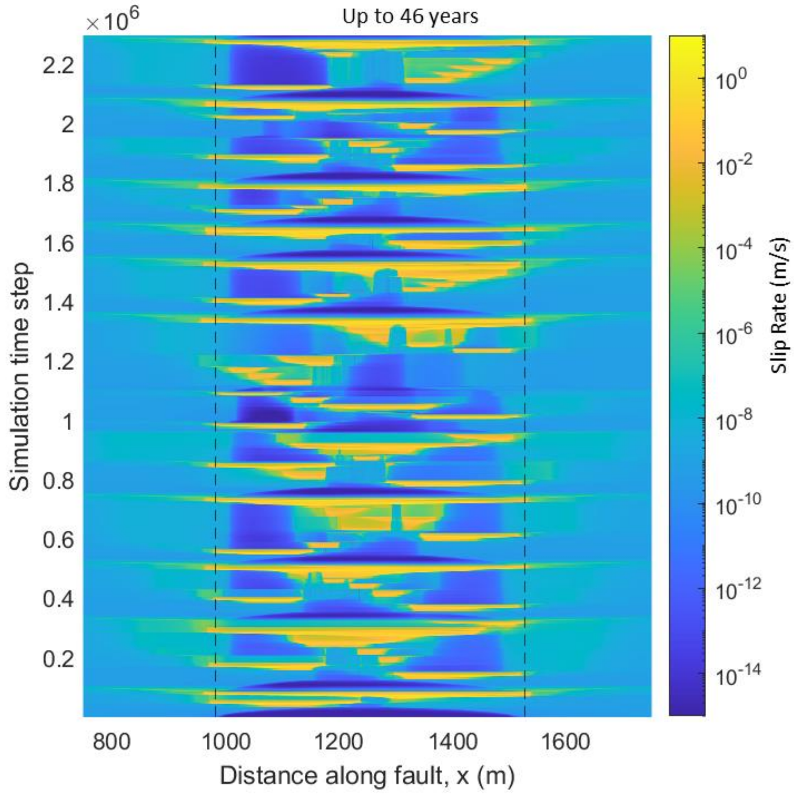

Figure S5. Long-term Spatio- temporal clustering of seismicity (yield strength, $\sigma_y = 36\ MPa$, viscosity, $\eta = 0.01\mu$). Partial rupture as well as occasional rupture spanning entire VW region persist throughout the simulation time. Same plot with results up to 25 years are shown in main text Figure-1b.

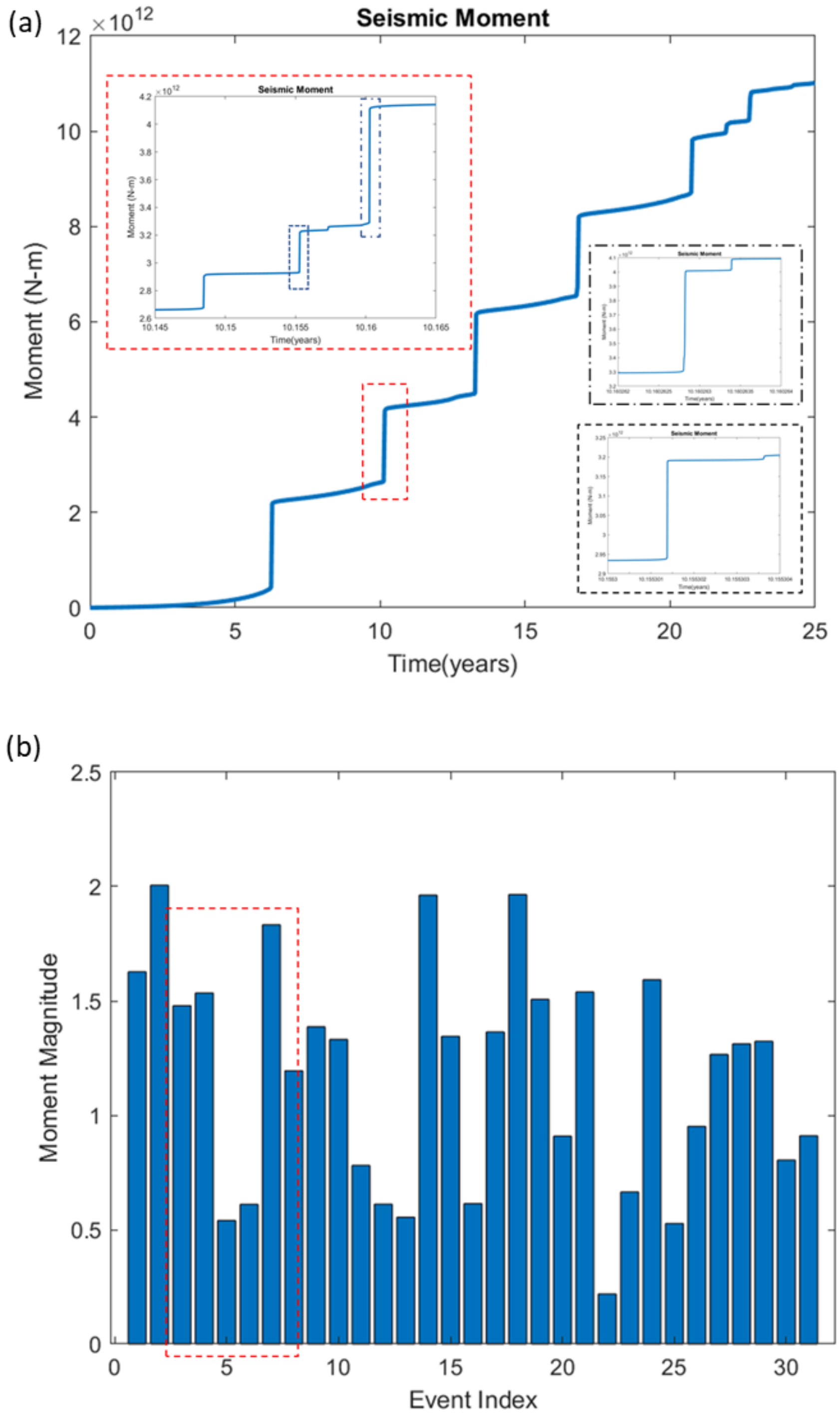

Figure S6. Seismic moment and magnitude of events for yield strength, $\sigma_y = 36\,MPa$, viscosity, $\eta = 0.01\mu$. (a) Time history of seismic moment computed with unit fault width. Zoomed-in view are shown in the insets for cluster-2. Sharp increase in moment happens during seisnmic slip. (b) Moment magnitude of the events that happened during 25 years. Largest magnitude found is $M_w \approx 2$. Magnitude of events in cluster-2 varies from $M_w = 0.5$ to $M_w = 1.8$.